NASA / TM—1999-208848

Experimental Determination of Load Carrying Capacity of Point Contact at Zero Entrainment Velocity

Bradley A. Shogrin
Case Western Reserve University, Cleveland, Ohio

William R. Jones, Jr.
Lewis Research Center, Cleveland, Ohio

Edward P. Kingsbury
IRC, Walpole, Massachusetts

Joseph M. Prahl
Case Western Reserve University, Cleveland, Ohio

January 1999

The NASA STI Program Office . . . in Profile

Since its founding, NASA has been dedicated to the advancement of aeronautics and space science. The NASA Scientific and Technical Information (STI) Program Office plays a key part in helping NASA maintain this important role.

The NASA STI Program Office is operated by Langley Research Center, the Lead Center for NASA's scientific and technical information. The NASA STI Program Office provides access to the NASA STI Database, the largest collection of aeronautical and space science STI in the world. The Program Office is also NASA's institutional mechanism for disseminating the results of its research and development activities. These results are published by NASA in the NASA STI Report Series, which includes the following report types:

- TECHNICAL PUBLICATION. Reports of completed research or a major significant phase of research that present the results of NASA programs and include extensive data or theoretical analysis. Includes compilations of significant scientific and technical data and information deemed to be of continuing reference value. NASA's counterpart of peer-reviewed formal professional papers but has less stringent limitations on manuscript length and extent of graphic presentations.

- TECHNICAL MEMORANDUM. Scientific and technical findings that are preliminary or of specialized interest, e.g., quick release reports, working papers, and bibliographies that contain minimal annotation. Does not contain extensive analysis.

- CONTRACTOR REPORT. Scientific and technical findings by NASA-sponsored contractors and grantees.

- CONFERENCE PUBLICATION. Collected papers from scientific and technical conferences, symposia, seminars, or other meetings sponsored or cosponsored by NASA.

- SPECIAL PUBLICATION. Scientific, technical, or historical information from NASA programs, projects, and missions, often concerned with subjects having substantial public interest.

- TECHNICAL TRANSLATION. English-language translations of foreign scientific and technical material pertinent to NASA's mission.

Specialized services that complement the STI Program Office's diverse offerings include creating custom thesauri, building customized data bases, organizing and publishing research results . . . even providing videos.

For more information about the NASA STI Program Office, see the following:

- Access the NASA STI Program Home Page at ***http://www.sti.nasa.gov***

- E-mail your question via the Internet to help@sti.nasa.gov

- Fax your question to the NASA Access Help Desk at (301) 621-0134

- Telephone the NASA Access Help Desk at (301) 621-0390

- Write to:
  NASA Access Help Desk
  NASA Center for AeroSpace Information
  7121 Standard Drive
  Hanover, MD 21076

NASA / TM—1999-208848

Experimental Determination of Load Carrying Capacity of Point Contact at Zero Entrainment Velocity

Bradley A. Shogrin
Case Western Reserve University, Cleveland, Ohio

William R. Jones, Jr.
Lewis Research Center, Cleveland, Ohio

Edward P. Kingsbury
IRC, Walpole, Massachusetts

Joseph M. Prahl
Case Western Reserve University, Cleveland, Ohio

National Aeronautics and
Space Administration

Lewis Research Center

January 1999

This report contains preliminary findings, subject to revision as analysis proceeds.

Available from

NASA Center for Aerospace Information
7121 Standard Drive
Hanover, MD 21076
Price Code: A03

National Technical Information Service
5285 Port Royal Road
Springfield, VA 22100
Price Code: A03

EXPERIMENTAL DETERMINATION OF LOAD CARRYING CAPACITY OF POINT CONTACTS AT ZERO ENTRAINMENT VELOCITY

Bradley A. Shogrin*
Case Western Reserve University
Cleveland, OH

William R. Jones, Jr.
NASA Lewis Research Center
Cleveland, OH

Edward P. Kingsbury
IRC
Walpole, MA

Joseph M. Prahl
Case Western Reserve University
Cleveland, OH

ABSTRACT

A capacitance technique was used to monitor the film thickness separating two steel balls of a unique tribometer while subjecting the ball-ball contact to highly stressed, zero entrainment velocity (ZEV) conditions. All tests were performed under a N_2 purge (R.H. < 1.0%) and utilized 52100 steel balls (R_a = 0.02 μm). Tribometer operations and capacitance-to-film-thickness accuracy were verified by comparing the film thickness approximations to established theoretical predictions for test conditions involving pure rolling. Pure rolling experiments were performed under maximum contact stresses and entrainment velocities of ≤ 1.0 GPa and 1.0 m/s to 3.0 m/s, respectively. All data from these baseline tests conformed to theory. ZEV tests were initiated after calibration of the tribometer and verification of film thickness approximation accuracy. Maximum contact stresses up to 0.57 GPa were supported at zero entrainment velocity with sliding speeds from 6.0 to 10.0 m/s for sustained amounts of time up to 28.8 minutes. The protective lubricating film separating the specimens at ZEV had a thickness between 0.10 and 0.14 μm (4 to 6 μin), which corresponds to an approximate Λ-value of 4. The film thickness did not have a strong dependence upon variations of load or speed. Decreasing the sliding speed from 10.0 m/s to 1 m/s revealed a rapid loss in load support between 3.0 and 1.0 m/s. The formation of an immobile film formed by lubricant entrapment is discussed as an explanation of the load carrying capacity at these zero entrainment velocity conditions, relevant to the ball-ball contact application in retainerless ball bearings.

Keywords: Zero entrainment velocity, elastohydrodynamic lubrication, retainerless bearing, capacitance technique

* Currently at Space Systems/Loral

INTRODUCTION

Every spacecraft uses momentum wheels or reaction wheels for the attitude control system (ACS). In principle, three wheels acting perpendicular to one another are adequate, but because of reliability problems, redundant wheels are included. In the past, gyro failures on Skylab (Ref. 1)and wheel anomalies (INSAT I-D, Superbird and Skylab) have shown that these precautions were well founded. One wheel on INSAT I-D had to be shut down. The operating wheels on INSAT and Superbird produced torque and vibration anomalies that compromised performance. An identical wheel design is being used on the GOES-NEXT series of weather satellites. If similar wheel anomalies occur on GOES, the imagery and sounding capability will be severely degraded. In addition, wheel anomalies on SOHO and AXAF spacecraft, have caused concerns.

Most failures and anomalies (high torque or torque noise), can be linked to the ball bearing retainers. Problems arise when the motion of the retainer becomes unstable. Retainer instabilities are characterized by large, erratic increases in driving torque, and large vibrations with accompanying loud noise, or squeal (Refs. 2 and 3). Kingsbury (Refs. 2 and 3) concluded that driving torque increases up to 300% can be attributed to retainer instabilities.

The retainer is usually made of a porous cotton phenolic material which is saturated with lubricant by vacuum impregnation. The resulting lubricant contained within the retainer is the only supply available to the bearing during the five to ten year orbiting life of the mechanism, other than the original charge of free lubricant.

Research at Aerospace Corp. (Refs. 4 and 5) has shown that cotton phenolic retainers, instead of supplying the bearing with oil, actually absorb oil from the bearing. Bertrand et al (Ref. 4) show that there is no net delivery of lubricant from a retainer to the metal parts of the bearing, even in a well lubricated bearing having a fully-impregnated retainer, and demonstrate that damage can occur to the bearing after the initial charge of lubricant on the metal parts begins to degrade.

Lubricant deprivation at the ball-retainer interface has been shown to cause retainer instability, leading to sporadic torque spikes and increased torque, and eventual bearing failure (Refs. 2, 6 and 7). Inconsistent lubricant flow from adjacent retainer pockets results in variable friction coefficients between the balls and the pocket throughout the bearing, which further fuels instabilities. Severe cases of lubricant deprivation at the pocket/ball interface results in substantial pocket wear (Ref. 7) which can result in catastrophic bearing seizure, and, more typically, hampers operations of the mechanism.

A radical solution to the crippling, retainer-related bearing instability problems is to eliminate the retainer. Kingsbury (Ref. 8) demonstrated that retainerless bearing assembly replacements for failed control moment gyroscopes (CMG) of Skylab, operated without compromise in a 13,000 hour ground-based life test. Retainerless bearing operation is questioned because of theoretical predictions of zero pressure generation, zero film thickness and zero load carrying capacity between neighboring balls in the bearing.

Theory

The skepticism surrounding retainerless bearings is well founded as the theoretical predictions by Hamrock and Dowson's (Ref. 9) expressions for minimum and central film thicknesses in fully flooded, isothermal elastohydrodynamic elliptical contacts are zero.

In a retainerless bearing assembly, the surface velocities of two neighboring balls at the point of contact are of the same magnitude but in opposite directions, and the entrainment velocity is equal to zero, yielding the prediction of zero film thickness. This is echoed in the predictions of the Reynolds equation. Since the entrainment velocity is zero at this point, the pressure gradient along the direction of motion is equal to zero, and therefore, the load carrying capacity is zero.

Summary of Previous Work Involving Zero Entrainment Velocity

Despite theoretical predictions of zero load carrying capacity, there is mounting evidence that a protective film is generated between two surfaces with equal and opposite peripheral velocities. The first such demonstrations occurred decades ago by both Cameron (Ref. 10) and Dyson and Wilson (Ref. 11) and utilized line contacts.

Cameron (Ref. 10) performed zero entrainment tests with dissimilar metals (steel/bronze) utilizing a disc machine with a line contact. The dissimilar-metal rollers performed without apparent scuffing until they seized at a maximum Hertzian contact stress (σ_{max}) of 0.44 GPa at a sliding speed of 2.1 m/s. However, when two case-hardened steel disks were run against one another, scuffing occurred almost immediately. It was concluded that the difference in the materials' thermal properties were responsible for the results and the "viscosity wedge" theory was proposed (Refs. 10 and 12). This theory is based upon viscosity variations induced by temperature gradients across the film. Since the thermal properties of the two steel rollers were identical, it was concluded that the thermal asymmetry necessary to form the oil film was not present and film formation was hindered.

Other researchers (Refs. 13 and 15) from that era confirmed that steel discs seized immediately at zero entrainment conditions, even when the "lightest" loads were applied. However, Dyson and Wilson (Ref. 11) demonstrated that two steel surfaces with a lapped finish ($R_a \approx 0.025$ μm), at zero entrainment velocity could support a σ_{max} of 0.7 GPa at sliding speeds ranging from ≈1 m/s to ≈ 8 m/s. No signs of scuffing were reported. These experiments cast doubt on the viscosity wedge theory proposed by Cameron, which has since been refuted (Ref. 16).

Dyson and Wilson (Ref. 11) suggested the previous failures experienced by other researchers (Refs. 10, 13 to 15) were due to the rough surfaces of the steel discs (presumed to be ground ($R_a \approx 1.0$ μm) rather than a lack of the proposed viscosity wedge. They proposed an alternative "viscosity wedge" theory. The principle of temperature dependence still remained in this theory, but instead of a temperature gradient across the film, the proposed temperature gradient occurred along the Hertzian zone on each surface, parallel to the direction of motion.

This theory is not well accepted because of its dependence upon large thermal gradients along the Hertzian contact length to form a protective film. In regards to both mechanisms, Dowson and Higginson (Ref. 17) conclude that neither can be expected to contribute significantly to the load carrying capacity of parallel surfaces. In fact, such viscosity wedge effects have been shown to reduce the load carrying capacity (Refs. 16 and 18).

Though left unexplained, Dyson and Wilson provided the only research demonstrating some form of load carrying capacity between highly stressed steel surfaces in line contact, maintaining ZEV. In more recent years, there has been growing evidence of a protective film separating two surfaces forming a point contact maintaining ZEV. This evidence comes from the successful demonstration of retainerless instrument bearings. Retainerless bearings have been operated by many researchers including; Kingsbury (Refs. 8, 19 to 27), Hunter (Ref. 28), Olson (Ref. 29), Schritz (Ref. 30), DeLucie (Ref. 31), and Jones (Refs. 32 and 33). This research represents thousands of hours of retainerless bearing operation without a single reported ball-ball failure. Rather, all noted failures occurred at the ball/race contacts. In fact, retainerless bearing operation has proven so reliable that other investigations of race/ball contacts have been performed utilizing their dependability (Refs. 19, 21, 25, 28 and 33).

In spite of these load carrying capacity demonstrations of point contacts subjected to ZEV, skepticism of its existence still prevails. The most definitive way to determine the existence of a load carrying capacity at a contact subjected to ZEV is to remove and isolate the point contact from all other surroundings and assumptions. A demonstration of film thickness at such conditions would indicate a load carrying capacity. Such work with sustained zero entrainment conditions using a point contact has never been attempted, and is the focus of the present study.

EXPERIMENTAL APPARATUS

Tribometer Overview

The tribometer used in this study is shown in Figure 1, and is briefly described below. A more detailed description of the tribometer and test procedures appears in Refs. 34 and 35. The tribometer is mounted on a vibration isolation table and enclosed in a plastic case which is constantly purged with N_2 to prevent oxidation of the lubricant and specimens. The tribometer is capable of subjecting its circular, point contact to a large array of elastohydrodynamic conditions, including; any combination of low to high rolling speeds (≈0.1 m/s to 10 m/s), light to heavy contact stresses (up to ≈4 GPa), pure rolling to any degree of slip, and steady to unsteady velocity fields. It is capable of simulating zero entrainment reversal, sustained ZEV, as well as impact loading.

The tribometer features two open faced, spindle units with high running accuracy. These spindle units hold the test specimen's contact pivot angle to $\approx 4 \times 10^{-4}$ degrees. Detail views of the spindle units and associated parts can be seen in Figure 2. Each unit is driven by a servo motor with encoder feedback (1000 counts/rev pre-quadrature, 4000 counts/rev post-quadrature). The film thickness of the lubricant between the test specimens is derived from capacitance measurements.

A bellows-based pneumatic loading system provides precise approach velocities and loading capabilities. The tribometer utilizes two Linear Variable Differential Transducers (LVDTs) to measure the relative linear displacement of the lower spindle support and the distance separating the test specimens. The two LVDTs have a nominal linear range and resolution of ± 0.625 mm (±0.025 in) and 25.4 μm (10 μin), respectively. The LVDTs are positioned collinear with the point of contact which is set as the midpoint. The average of the LVDT readings is taken as the ball-ball separation distance.

All instrumentation and functions of the tribometer are simultaneously controlled and monitored with a LabVIEW-based computer data acquisition (DAQ) system. The DAQ system automatically shuts down all operations, separates the specimens, and stops shaft rotation when user-defined limit criteria have been surpassed, preventing scuffing of the test specimens. Data is recorded into an ASCII file and seen in real time as the test progresses.

Test Specimens

Test specimens were 0.064 m (2.50 in) diameter through hardened AISI 52100 steel (Rockwell C62) grade 100 balls, with an arithmetic surface roughness average, R_a, of 0.02 μm (0.8 μin). Special care was made not to damage or modify the crown while machining the balls. The resulting machined specimens had surface finish, surface metallurgy, and curvature that mimicked balls typically used in high precision bearings.

Spindle Units

Two spindle units were custom built using high precision spindle design practices and tolerances set forth by SKF (Ref. 36). Each unit has a runout of ≈2.5 μm (100 μin) and is electrically isolated from ground to assure accurate capacitance measurements.

Capacitance Measurements

The capacitance, resistance, and dissipation values of the lubricating film are monitored with a HP4263A LCR meter. For the test conditions used, the instrument has a measurement accuracy of ±0.4% for capacitance and ± 0.004 for dissipation.

The electrical connections to the rotating reference frame are made through two mercury, triple sealed slip rings (one on each axis). A wire extends along the rotation axis from the slip ring through the electrically-isolating couplings (Figure 2) and connects to the shaft.

Closed Loop Loading Mechanism

Precise displacement of the lower support and contact loading is provided by a closed loop, pneumatic loading system. The loading system is updated every ≅ 250 ms using an iterative loop in the DAQ software program. Ball-ball approach velocities and loading rates as low as, but not limited to, 12.5 nm/sec (0.5 μin/sec) and 0.022 N/sec (0.005 lbf/sec), respectively, were obtained using this unique loading technique.

Lubricant

A filtered polyalphaolefin (PAO-182), fortified with an antiwear additive (tricresyl phosphate) at 1.0 wt.% and an antioxidant (hindered phenol) at 0.5 wt %, was used. Physical properties are shown in Table 1. Similar PAOs of various molecular weights were used in the retainerless bearing studies (Refs. 21, 29, 41 and 32).

The dielectric breakdown voltage, or dielectric strength, of 13.8 Volts/μm used for the test lubricant is that of a similar PAO lubricant (none was given for the test lubricant). Assuming the contact is free of conductive contaminants, the dielectric strength on a microscale is equal to 13.8 V/μm (0.350V/μin). The effective pressure-viscosity coefficient, α_{EFF}, of the test lubricant was determined by Smeeth and Spikes (Ref. 38) at four temperatures (24, 40, 80, and 120 °C) using ultrathin film interferometry and are summarized in Table 2. These values were produced using a σ_{max}, of 0.54 GPa, and have an accuracy of ± 1.0 GPa^{-1}.

The lubricant was supplied to the contact point one of two ways. It was either drawn into the contact area by the lower ball which was partially submerged in a 200 ml lubricant bath, or it was injected into the contact area at a rate of $\approx$ 1 ml/sec. At higher rotation speeds, the submersion technique was limited by air film formation between the stationary lubricant in the bath and the moving lubricant on the specimen.

The temperatures of both the bath and meniscus region were monitored. As seen in Figure 2, a thermocouple (with an accuracy of ± 1 °C) was submerged in the bath. An IR pyrometer with a resolution of ± 1 °C was focused on the meniscus region and had a ≈1 mm spot size.

EXPERIMENTAL PROCEDURES

Specimen Preparation Prior to Testing

Prior to spindle assembly, test specimens were ultrasonically cleaned in hexane, acetone, and finally methanol for 20 minutes each. Before initial testing, the test specimens were wiped down with a lent-free cloth containing each of the three solvents. Specimens were allowed to dry in the enclosed N_2 atmosphere and coated with the test lubricant. Testing was initiated thereafter, and surfaces were not subsequently cleaned. All tests were run using the same test specimens.

DAQ Limit Criteria Selection

Adequate limit criteria were implemented in the DAQ automatic shutdown procedures to assure the health of the test surfaces before subjecting them to potentially damaging conditions. For a full explanation of the limit criteria see Reference 34.

Pure Rolling Tests

Tests were performed to determine the EHD film thickness separating a loaded contact subject to pure rolling conditions. These results would be compared to well established, theoretical film thickness predictions to verify the capacitance-to-film-thickness model. Pure rolling tests were characterized by giving each test specimen equal peripheral velocities. Limit criteria for all pure rolling tests were: a capacitance maximum of 25 pF, a resistance minimum of 500 Ω, a maximum dissipation factor of 0.5, and maximum lubricant bath and inlet temperature of 35 °C. The LabVIEW software program automatically shutdown all operations if one of the following occurred: either the capacitance or resistance criteria was exceeded two consecutive times, the dissipation factor was exceeded three consecutive times, or either temperature limit was exceeded once.

Pure rolling tests were performed by bringing the motors up to speed prior to contact. The specimens were slowly brought together at a rate of 2.3 μm/sec (90 μin/sec). Shaft rotation and limit-enabling occurred at a surface separation distance of ≈180 μm (0.007 inches), as the surfaces continued their approach. After the rotating surfaces came into contact, the contact load increased to its final desired value at a rate of ≈0.45 N/sec (0.1 lbf/sec).

The test conditions of pure rolling experiments appear in Table 3. Three σ_{max} were used, 0.64, 0.81 and 1.0 GPa, at entrainment velocities from 1.5 to 3.0 m/s. The entrainment velocity was changed periodically throughout a given test. Other experiments involving slip under similar contact stresses and entrainment velocities are described elsewhere (Refs. 34 and 35).

Zero Entrainment Tests

ZEV tests were initiated after qualifying the tribometer and film thickness approximation technique. Approach velocity ranged from 2.3 μm/sec (90 μin/sec) to 0.05 μm/sec (2.0 μin/sec).

The tests at ZEV can be separated into two categories: exploratory and conclusive. Exploratory tests were performed to gain experience and expectations of later testing. Exploratory tests were used to determine what approach velocities, failure limits, shaft rotation speeds and general running conditions to use for later tests. An important goal of the exploratory tests was to explore these conditions without contact failure. Therefore, they were operated with conservative running conditions. As more experience was gained, the test conditions needed to maintain a sustained load carrying capacity became apparent. The tests gradually made the transition from exploratory to conclusive. The conclusive tests are so named because they conclusively demonstrated that the highly loaded contact can support a load at ZEV for a sustained amount of time without contact failure.

A total of twenty-five (25) tests were run at ZEV. The pertinent running conditions of these tests are displayed in Table 4. These tests are numbered in time sequential order. The sliding speed is equal to the difference of the peripheral velocities. The last five columns list the particular limit criteria and the number of consecutive times it had to be surpassed

(in parenthesis) before automatic shutdown. The temperature values needed to be surpassed only once before shutdown was initiated.

RESULTS

Capacitance to Film Thickness Approximation

The capacitance-to-film-thickness approximation is detailed elsewhere (Ref. 34). The approach was first used by Dyson et. al (Ref. 39) for line contacts. A similar model was derived by Allen et. al (Ref. 40) for elliptical contacts and used by Kingsbury et. al (Ref. 25)and Hunter (Ref. 28).

Briefly, the capacitance model consists of two parts, C_{hertz} and $C_{meniscus}$. Where C_{hertz} is the capacitance of the Hertzian area, $r \le r_{hertz}$: and $C_{meniscus}$ is the capacitance of the area surrounding the Hertzian area, $r_{hertz} < r < \infty$, which is taken as the circular area of the lubricant meniscus. The meniscus term encompasses both the inlet and outlet regions, and the surrounding side regions. The capacitance model is shown below with all terms included.

$$C_{total} = C_{hertz} + C_{meniscus}$$

$$C_{total} = \left[\frac{\varepsilon_{hertz} A_{hertz}}{4\pi\kappa h_{film}}\right] + \int_0^{2\pi}\int_{r_{hertz}}^{r}\left[\frac{\varepsilon_{atm} r}{4\pi\kappa\left[2\left[\left(\sqrt{R^2 - r_{hertz}^2}\right) - \left(\sqrt{R^2 - r^2}\right)\right] + h_{film}\right]}\right] dr d\theta$$

In previous work (Refs. 34 and 35) the dielectric constant of the lubricant at atmospheric pressure, ε_{atm}, and at Hertzian pressures, ε_{hertz}, were found to be 2.6 and 3.0, respectively. Therefore, all of the above parameters are either constants (ε_{atm}, ε_{hertz}, R, κ), measured quantities, (C_{total}, in pF), or calculated from the load (A_{hertz}, r_{hertz}), leaving the film thickness, h_{film}, as the only unknown. The h_{film} was calculated by setting the above equation to zero and solving for the root using the secant method for each capacitance/load data pair while varying h_{film} until the expression was equal to zero. The final value of h_{film} was the root of the equation, and thus the film thickness corresponding to the capacitance/load pair. Each data point was calculated with the capacitance and load at that respective time, and represents an independent calculation. Raw capacitance values were smoothed (data width of 15 points) to see the general data trends more clearly using a standard smoothing technique. A running median smoother was used which also computed and smoothed the residuals and added the two smoothed vectors (Ref. 34).

Pure Rolling Tests

These tests were performed by bringing the motors up to speed prior to contact, as the lower test specimen slowly approached the upper test specimen. The approach and entrainment velocity (multiplied by a factor of 100) for test "3rwos" appears in Figure 3. Each plot contains approximately 2000 individual data points. The figure shows the lower specimen approaching the upper specimen at a rate of 2.68 μm/sec (106 μin/sec). This is the average of the two LVDT readings, which typically fluctuated no more than ≈20 μm (800 μin) from one another. The

motors were enabled at 2115 seconds, just prior to the onset of ball-ball loading. Loading began at ≈2190 seconds and is signified by the abrupt change in LVDT data. At that time, the vertical movement of the lower specimen was restricted by the rotating upper specimen and the specimens began to load against one another. This was driven by the constant increase is proportional to the valve voltage sent from the DAQ program as it continuously attempted to satisfy the desired load requirement. The voltage increment remained unchanged at 0.0005V, resulting in a load rate of ≈0.45 newton/sec (0.1 lbf/sec). The test was manually shutdown at ≈2690 seconds.

The entrainment velocity was first set to 2.5 m/s. After ≈200 seconds the entrainment velocity was changed to 3.0 m/s, where it stayed for ≈100 seconds before being changed to 2.0 m/s. Acceleration and deceleration rates remained constant throughout all testing at 0.5 rps^2.

The associated film thickness approximations obtained with the secant method using capacitance values are shown in Figure 4, along with the theoretical minimum, h_{min}, and central film thickness, h_{cent}, calculations at room temperature (24 °C) calculated with Hamrock and Dowson's equations (Ref. 9). This value was chosen because the temperature of both the meniscus and lubricant bath only rose between 1 °C and 4 °C for all tests involving pure rolling. These rises are expected, as the entrainment velocities used in these tests (≤ 3.0 m/s) were too small to induce appreciable inlet heating.

As seen in Figure 4, both the theoretical and calculated film thicknesses decreased as the two test specimens began to load against one another at ≈2190 seconds with a constant entrainment velocity of 2.5 m/s. As the desired load was reached, all three calculations leveled out until the entrainment velocity increased to 3.0 m/s at ≈2360 seconds, thus increasing the film thickness. At ≈2460 seconds the entrainment velocity decreased to 2.0 m/s, decreasing the theoretical and calculated film thicknesses.

In a typical EHL point contact the Hertzian contact consists of two regions: a crescent-shaped region of minimum film thickness, and the larger remaining area of the contact with relatively constant film thickness, designated the central film thickness. Since the model used in this study does not make this distinction, it is reasonable to assume that the calculated film thickness should lie somewhere between the theoretical minimum and central film thicknesses.

The film thickness approximations of the remaining pure rolling tests also corresponded well with theory and are summarized in Table 5. This table contains the mean and standard deviation of all data points collected for smoothed capacitance values ($Capacitance_{mean}$ and $Capacitance_{StandDev}$), associated h approximations (h_{mean} and $h_{StandDev}$), and h_{min} and h_{cent} calculated at 24 °C ($minimum_{24C}$ and $central_{24C}$). The number of data points collected for each segment are also tabulated (*number of data points*). The calculated h agree well with h_{min} and h_{cent}. All of the mean experimental approximations lie within the theoretical h_{min} and h_{cent} approximations.

Zero Entrainment Velocity

A total of twenty-five tests were performed at ZEV. Nine of these tests violated limit criteria at the onset of ball-ball loading and shutdown automatically. Nine of the tests supported a small load for an extended period of time (from 15 seconds to 9.6 minutes) prior to shutdown. Five tests demonstrated a sustained lubricant film under substantial load. The final two tests were performed at lower speeds (3.0 m/s and 1.0 m/s) with the same limit criteria to determine the speed and load dependency upon successful zero entrainment operations. After each test, both surfaces were checked with the naked eye for signs of damage. Damage was not observed throughout testing. One of the specimens was removed after testing and observed under an optical microscope.

The first test, *1z*, used a sliding speed of 5.0 m/s sliding speed, well within the range of ball-ball sliding speeds used in the retainerless bearing work performed by Kingsbury (Ref. 20), DeLucie (Ref. 31) and Olsen (Ref. 29). The approach velocity of this first test (2.3 μm/sec) was chosen to reflect the belief that a slow approach velocity is superior to a rapid approach. This is especially true if a polymerized or other protective film must form at the contact to prevent failure. The failure limits used for the first test were those of the pure rolling experiments, but only needed to be surpassed once to initiate automatic shut down. This test shut down immediately at the onset of ball-ball loading. Over the next few tests, the approach velocity became the focus. Eventually, the final approach velocity was maintained at 0.05 μm/sec for all zero entrainment velocity tests and attention focused on the limit criteria and the number of consecutive times that these needed to be surpassed to initiate shutdown. Shutdown criteria, limits, and consecutive times, were relaxed to the point that load carrying capacity at ZEV under substantial stresses was demonstrated.

Conclusive Zero Entrainment Velocity Tests

The zero entrainment tests that demonstrate sustained load carrying capacity at elevated contact stresses are summarized in Table 6. Test “22z” sustained load for the longest time at the second highest load and was manually shutdown after 28.8 minutes of operation at a maximum contact stress of 0.52 GPa. A total of 4311 data sets were collected while the contact was loaded. The mean capacitance and calculated h_{film} were 21.8 pF and 0.143 μm (5.6 μin), respectively.

The five test durations ranged from 17.5 minutes to 28.8 minutes with σ_{max} from 0.35 to 0.57 GPa, and sliding velocities from 6.0 to 10.0 m/s. Two of the tests were manually shutdown, after these tests had shown adequate sustained load carrying capacity at zero entrainment velocity. Two tests, “19z” and “23z,” shutdown due to IR temperature violation. Test “20z” was shutdown due to five consecutive capacitance violations. Capacitance violations do not necessarily indicate metal-metal contact, and could result from dielectric breakdown under very thin film conditions, or electrical noise, which has been shown to be a problem for faulty capacitance values (Ref. 34). For the test lubricant, dielectric breakdown occurs for h_{film} equal to or less than ≈0.04 μm (1.4 μin). Dielectric breakdown is plausible given the calculated mean film thicknesses of 0.107 μm (4.2 μin).

An important conclusion from these tests is that h_{film} was not affected by varying the sliding velocity. Since the lubricant was not entrained into the contact in these tests, it is reasonable that a speed dependence was not observed, and the film separation of the specimens must be caused by means other than hydrodynamic.

Graphical Representation of Zero Entrainment Testing

The approach and load bearing portion of test "21z,"as monitored with the LVDT average, is seen in Figure 5. The approach velocity of 0.066 μm/sec (2.6 μin/sec) was driven by the closed loop loading algorithm set here at a proportional valve voltage increment of 0.00001V. The valve voltage and contact stress are presented in Figures 6 and 7, respectively.

During the approach, the voltage to the pneumatic valve increased at a constant rate to reach the desired contact stress. Once the actual stress was within the desired range, the voltage increment ceased (starting at 1745 seconds), until the effects of thermal expansion induced by the constant, linear rise in contact temperature caused additional loading between the two specimens due to thermal expansion (Figure 5). Starting at 1860 seconds, the closed loop algorithm began a voltage decrement to maintain the desired stress of 0.34 GPa. The desired stress was increased to 0.43 GPa (± 0.01 GPa) at 2033 seconds, causing the voltage increment to increase. The voltage again decreased starting at 2240 seconds, as the specimens continued to expand thermally, inducing additional loads on the contact. This process continued throughout the test until it was shutdown manually after 26.7 minutes of sustained load carrying capacity at zero entrainment velocity.

The calculated h_{film} corresponding to the smoothed capacitance values are presented in Figure 8. The mean and standard deviation of the capacitance values during loaded contact were 21.8 pF and 1.1 pF, respectively. The h_{mean} value during this time is 0.14 μm ± 0.02 μm (5.4 μin ± 0.8 μin), which corresponds to a Λ-value ≈5.

Remaining Zero Entrainment Tests

Table 7 presents the results of other tests that demonstrate moderate load carrying capacity at ZEV. The maximum contact stress ranged from 0.35 GPa (contact load of 1.0 lbf) to 0.15 GPa (contact load of 0.1 lbf). The approximate temperature rise of the meniscus and bath are also listed, as is the surpassed limit criteria which prompted automatic shutdown.

Table 8 contains tests that demonstrate moderate load carrying capacity at various contact stresses and sliding speeds. All tests in Table 8 used the same limit criteria shutdown protocol. The contact load of tests 24z and 25z was continuously increased at a rate of 0.022 N/sec until the limit criteria were surpassed. In test 25z, the capacitance, resistance, and dissipation limit criteria were all surpassed at the onset of loading.

The remaining tests (1z-4z, 6z, 7z, and 12z-14z) surpassed the limit criteria immediately upon the onset of contact and shutdown automatically, verifying shutdown capabilities of the DAQ software prior to contact failure.

DISCUSSION

Overview

The presence of a sustained film thickness separating two heavily stressed steel balls, forming a point contact at ZEV, has been measured. The possibility of a squeeze film supplying the demonstrated protection is considered. Optical microscopic observations of the Hertzian zone after testing, coupled with the magnitude of film thicknesses measured in the zero entrainment velocity tests, suggest a surface layer supplying the demonstrated protection at ZEV.

Squeeze Film Analysis

The test spindles had a runout of ≈ 2.5 μm (100 μin) at the point of contact. The runout of the surfaces resembles two cams in contact. The rotational center of the lower specimen (upper specimen fixed) can do one of two things; it could remain stationary, or, it could move up and down at a frequency equal to the shaft rotational frequency. If the specimen's center of rotation remains relatively fixed, a squeeze film phenomenon may explain the results. If the lower surface follows the upper surface, maintaining a constant distance between them, it would negate the possibility of squeeze film formation.

A number of tests were performed while sampling the load cell's analog output with the FFT analyzer (Ref. 34). This data indicated that the surfaces followed one another, leaving a constant distance between them, negating the possibility of a squeeze film.

Optical Microscopic Observations of the Test Surface

After completion of all tests (zero entrainment as well as roll with/without slip), the lower test specimen was removed from its spindle unit and inspected under a low power optical microscope. Small, superficial scratches within the Hertzian region were observed. The width of the scratches ranged from ≈0.01 mm to ≈0.001 mm, with a typical value of ≈0.005 mm. The length of the scratches ranged from ≈0.50 mm to ≈0.01 mm, with a typical value of ≈0.3 mm. These scratches were probably formed when an occasional asperity "broke through" the protective film or by particles within the oil. Such scratches would be a length equal-to, or less than two Hertzian diameters (max. Hertz diameter of zero entrainment test = 0.26 mm).

Actual scratch lengths in the present study agree well with the above analogy and proposed method of scratch formation. Given the small number of scratches present (≈100 around ball), the frequency of such occurrences are low considering that each shaft rotated a total of 168,000 times during the heavily loaded zero entrainment tests represented in Tables 6 through 8. The presence of some superficial scratching indicates that the protective film is thin and that asperities (particles) occasionally penetrate.

Surface Damage of Previous Work Relative to the Present Experiments

The success or failure of earlier experiments involving steel against steel disc machines under zero entrainment conditions strongly depended upon the surface finish of the test specimens. Dyson and Wilson (Ref. 11) were the first to successfully demonstrate a substantial load carrying capacity between two lapped steel surfaces ($R_a \approx 0.025$ μm) in a line contact under such conditions and concluded scuffing did not occur. However, means other than visual inspection were not mentioned.

Cameron's (Ref. 10) and others (Refs. 13 to 15) experience with rougher steel surfaces (assumed $R_a \approx 1.0$ μm) subject to ZEV was not as promising. Even the lightest loads resulted in scuffing and failure of the ground (presumably) surfaces.

The first investigation of the load carrying capacity of a point contact maintaining was performed by Kingsbury (Ref. 20). He used a small (11.08 mm pitch diameter) retainerless angular contact bearing (440C steel balls and races) in which the inner and outer races were independently driven in opposite direction so that the ball centers remained stationary. Maximum ball-ball stresses in excess of 1.0 GPa were realized with three lubricants, a mineral oil, a traction fluid, and n-hexadecane, at ball-ball sliding speeds of 7.8 m/s. Severe scuffing resulting in bearing failure was present on balls lubricated with both the traction fluid and hexadecane. The ball-ball stress of the test lubricated with mineral oil was presumably limited by the size of the driving motor. The scuffing has yet to be explained.

Kingsbury's work was extended by Olson (Ref. 29) and DeLucie (Ref. 31) who used two similar test rigs to perform tests with 52100 steel balls and races (R_a of≈0.02 μm), lubricated with a variety of lubricants (two polyalphaolefins (PAO), two mineral oils, hexadecane, and a perfluoropolyether). In addition, the effects of various pre-cleaning procedures were investigated by Olson and found to have significant impact on bearing health. All bearings Olson tested pre-cleaned in an alkaline solution, as opposed to the standard 3-solvent method (toluene, Freon, methanol) failed. Alkaline cleaning is considered much more aggressive than the three-solvent cleaning technique because it is capable of removing a larger fraction of organic species from the surface. Alkaline cleaning has even been shown to remove highly bound inorganic $FePO_4$ films from bearing surfaces (Ref. 41) ($FePO_4$ is an antiwear coating formed by tricresylphosphate (TCP) pretreatment). The fact that the cleaning technique has a profound effect supports the belief that surface chemistry plays an important role. The remaining tests in both studies were cleaned using the 3-solvent method.

Maximum ball-ball contact stresses of between 0 GPa and ≈1 GPa were obtained using sliding speeds ranging from 2.3 to 25.5 m/s. All successful tests resulted in either light scratching or a "frosted appearance" at the ball-ball locus on nearly every ball. These scratches were considered superficial, and were only observable with an optical microscope. The ball-ball superficial damage was not found to depend upon sliding speed, contact stress or lubricant type, and never resulted in distress while running. An explanation of the superficial ball-ball contact surface scratches is still sought.

Boundary Film Phenomena

The presented lubricating ability and load carrying capacity at ZEV is thought to be a boundary film phenomenon. Standard EHL theories are ill-equipped to model such films, as the equations are founded upon continuum assumptions. Although, a definitive explanation for the exhibited surface protection is still sought, there are plausible arguments. Recent work in the advancing field of ultrathin lubrication indicates the presence of highly tenacious, immobile films present in EHL contacts at low rolling speeds. Additionally, it is plausible that the reactive film produced by the TCP additive enhances the observed protection. An extended immobile film may explain the protection and demonstrated load carrying capacity at ZEV.

Additive Boundary Film Formation

The lubricant used in this study was fortified with tricresyl phosphate (TCP) which plays a significant role in the boundary lubrication performance. It is believed that this additive forms a surface film, which is partially a reactive layer consisting of iron phosphate ($FePO_4$) and a strongly adsorbed layer comprised of phosphate derivatives (Ref. 41). Since thin layers (≤ 0.01 μm thick) form only at elevated temperatures, they typically develop at the contact while in boundary lubricated conditions, where temperatures at the asperities (Ref. 42) are sufficiently high to promote film formation. The conditions used in these studies would supply enough local asperity energy to fuel sufficient iron phosphate ($FePO_4$) boundary layer formation as it is appreciable to induce rapid reaction rates. However, although TCP is an extremely effective additive, few would argue that the surface protection it provides could solely account for the exhibited load carrying capacity at zero entrainment velocity. Additionally, Delucie and Olson's successful experiments with unformulated lubricants further suggests a more complex mechanism of surface protection.

Thick Immobile Layers

Earlier work (Refs. 43 to 45) indirectly demonstrated the presence of chemically adsorbed, multimolecular films whose properties vary from that of the bulk liquid. Immobile layer formation was demonstrated by Fuks (Ref. 45) as he showed that two loaded parallel flat steel discs submerged in various mineral oils remain separated by a thin layer of oil even after several hours under load.

More recently, Georges et. al (Ref. 46) detected the presence of immobile films approximately two to ten molecular layers thick in static squeeze film tests. These immobile films were said not to participate in the hydrodynamic flow of the fluid, and were detected on all substrates tested, including mica, cobalt, gold, platinum, and steel. Various fluids were tested including n-dodecane, n-hexadecane, a nonane, a pentane, and a siloxane. The fact that these immobile films were present on such a variety of substrates using such a diversity of fluids suggests that immobile surface layers are not uncommon. These findings are supported by others (Ref. 47) who also describe immobile surface film formation using a similar force balance technique. However, these experiments were performed with very little contact stress, and without relative motion.

Recent studies (Refs. 38, 48 to 50) have utilized ultrathin film interferometry to investigate immobile surface film formation in EHD contacts. Spikes et. al (Ref. 48) detected the presence of "immobile" surface films up to 20 nm (0.8 μin) thick when using rolling speeds from 0.0002 m/sec to 0.1 m/sec, and σ_{max} of 0.45-0.52 GPa, and with various lubricants containing polymer blends. These films had a much higher viscosity than the bulk lubricant, producing thicker films than predicted using the bulk lubricants' viscosity (Ref. 49). These immobile films had a thickness independent of entrainment velocity and slowly squeezed out from the heavily stressed contact once motion had ceased (Ref. 48). As speeds increased, a conventional EHD film was produced whose thickness was based upon the bulk properties of the oil and is "superimposed on the immobile film" (Refs. 48 and 49). Immobile film formation was found to be independent of temperature as it was detected on surfaces which had been tested at temperatures between 20 and 120 °C (Ref. 49).

Since these immobile lubricant layers slowly squeezed out after motion had stopped, Cann and Spikes (Ref. 48) postulated that the rolling motion trapped these films, which could not be displaced by viscous flow within the time it took the contact to confine it. After the rolling motion had stopped, there was plenty of time for these polymers to sufficiently untangle and squeeze out of the contact. This strongly suggests a time factor in immobile layer formation. In order to perform their experiments, Spikes et. al (Refs. 38, 48 to 50) obviously had to slow the rolling speed down, which allowed plenty of time for the majority of polymer to viscously move aside before being entrapped. One might argue that the thickness of the polymer-entangled boundary film increases as the entrapment time decreases. Thus, thicker immobile boundary layers could form at significantly lower entrapment times, such as the conditions used in this study, regardless of entrainment velocity.

The work here suggests that there is a critical speed/contact stress relationship (Table 8) corresponding to a critical entrapped, entangled, immobile boundary film that is capable of sustaining a load carrying capacity. Past this thickness, the lubricant behaves as one might expect it to, and standard EHL assumptions can be applied. The speed independence demonstrated at higher sliding speeds (6.0 m/s to 10.0 m/s) also occurred in the work by Olson (Ref. 29) and DeLucie (Ref. 31).

As the sliding speed was continuously decreased (down to 1.0 m/s in this work), the load the protective film could support also decreased. Of course, if the sliding speeds in these experiments approach zero, the contact would be modeled as the trivial case of two stationary spheres in contact. This stationary case resembles the work of Georges (Ref. 46), Israelachvili (Ref. 47) and Cann (Ref. 48) in which the immobile films eventually squeeze out, leaving metal-metal contact and inevitable bearing failure.

It is possible that the boundary film formation demonstrated in this work at ZEV is of an immobile nature, built up to a certain critical thickness by lubricant entrapment. Immobile film formation could explain the protection seen in retainerless bearings during start-up and shut-down. In this study, the protective boundary film could have further been aided by $FePO_4$ boundary layer formation from the TCP additive.

SUMMARY OF RESULTS

1. A unique test facility was utilized to determine the existence and magnitude of a lubricating film at a point contact subjected to sustained zero entrainment velocity (ZEV) and highly stressed conditions.
2. The accuracy of the capacitance-to-film thickness determinations were verified by comparing them to known, well established theoretical predictions for pure rolling conditions.
3. Despite contrary theoretical predictions, substantial, sustained load carrying capacities were demonstrated at ZEV without damage to the surfaces. Maximum Hertzian contact stresses up to 0.57 GPa were supported, at sliding speeds ranging from 6.0 m/s to 10.0 m/s, for sustained periods of time.
4. The film thickness remained relatively constant during any particular test as the contact stress was increased from near 0 GPa to values approaching 0.6 GPa. Likewise, the film thickness had little variation as the sliding speed was varied between tests from 6.0 to 10.0 m/s.
5. As the sliding speed was decreased to 3.0 m/s and again to 1.0 m/s, a critical speed/contact stress relationship emerged. As sliding speed decreased the load the protective film can support also decreased.
6. The lubricating film that separated the specimens at ZEV had an approximate thickness between 0.10 and 0.14 μm (4 to 6 μin), corresponding to a lambda value of ≈ 4, which describes a contact in mixed lubricating conditions.

CONCLUSION

A boundary film exists in concentrated contacts under zero entrainment conditions which protects the surfaces from damage and allows for some load carrying capacity. Its mechanism of generation is not known.

REFERENCES

1) "Proceedings of the Committee to Investigate the Skylab CMG No. 2 Orbital Anomalies," George C. Marshall Space Flight Center, (January 1974).

2) Kingsbury, E., "Torque Variations in Instrument Ball Bearings," *ASLE Transactions*, **8**, 435-441, (1965).

3) Kingsbury, E. and Walker, R., "Motions of an Unstable Retainer in an Instrument Ball Bearing," *Journal of Tribology*, **116**, 202-208, (April 1994).

4) Bertrand, P.A., Carré, D.J. and Bauer, R., "Oil Exchange Between Ball Bearings and Cotton-Phenolic Ball-Bearing Retainers," *Tribology Transactions*, **38**, 2, 342-352, (1995).

5) Bertrand, P.A., "Oil Absorption into Cotton-Phenolic Material," *J. Mater. Res.*, **8**, 7, 1749-1757, (July 1993).

6) Loewenthal, S., Boesinger, E.A., and Donley, A.D., "Observations of Cage Instability," *Proc. of the DOD/Instrument Bearing Working Group Intl. Rolling Element Bearing Symp.*, (1991).

7) Gupta, P.K., "Frictional Instabilities in Ball Bearings," *Tribology Transactions*, **31**, 2, 258-268, (1988).

8) Kingsbury, E., "Large Bearing Operation Without Retainer," *Lubrication Engineering*, **35**, 9, 517-520, (1979).

9) Hamrock, B.J. and Dowson, D., Ball Bearing Lubrication. The Elastohydrodynamics of Elliptical Contacts, John Wiley and Sons, Inc., (1981).

10) Cameron, A. "Hydrodynamic Lubrication of Rotating Disks in Pure Sliding. A New Type of Oil Film Formation," *Jr. Inst. of Petroleum*, **37**, 471-486, (1951).

11) Dyson, A. and Wilson, A.R., "Film Thicknesses in Elastohydrodynamic Lubrication at High Slide/Roll Ratios," *Proc. Inst. Mech. Eng*., 183, Part 3P, 81-97, (1968-1969).

12) Cameron, A., "The Viscosity Wedge," *ASLE Trans.*, **1**, 248, (1958).

13) Merritt, H.E., "Worm Gear Performance," *Proc. Instn. Mech. Engrs.*, **128**, 127, (1935).

14) Misharin, Yu., A., and Sivyakova, A.V., "A Laboratory Study of Anti-Seizure Properties of Certain Materials Used for Worm Gears," Nat. Res.Council of Canada, *Tech. Trans*., No. TT-1058, (1963).

15) Blok, H., "Gear Wear as Related to Viscosity of Oil," *Mechanical Wear*, Proc. Conf. M.I.T., Cambridge, Mass, (June 1948).

16) Cameron, A. "New Theory for Parallel Surface Thrust Bearing," *Engineering*, **190**, 904, (1960).

17) Dowson, D., and Higginson, Elastohydrodynamic Lubrication, SI Edition, Oxford, Pergamon Press, (1977).

18) Dowson, D. and Hudson, J.D., "Thermohydrodynamic Analysis," *Inst. Mech. Eng. Lubn. Conf*., 45-51, (May 1963).

19) Kingsbury, E.P., "Lubricant-Breakdown in Instrument Ball Bearings," *Journal of Lubrication Technology*, **100**, 386-394, (July 1978).

20) Kingsbury, E., "Ball-Ball Load Carrying Capacity in Retainerless Angular-Contact Bearings," *J. Lube. Tech*., **104**, 327-329, (1982).

21) Kingsbury, E., “Influences on Polymer Formation Rate in Instrument Ball Bearings,” *Tribology Transactions*, **35**, 1, 184-188, (1992).

22) Kingsbury, E., “Basic Speed Ratio of an Angular Contact Bearing,” *Journal of Lubrication Technology*, **102**, 391-394, (July 1980).

23) Kingsbury, E., “Slip Measurement in an Angular Contact Ball Bearing,” *Journal of Lubrication Technology*, **105**, 162-165, (April 1983).

24) Kingsbury, E., “Dynamic and Coupling Influences on Basic Speed Ratio of an Angular Contact Bearing,” *Wear*, **63**, 189-196, (1980).

25) Kingsbury, E., Schritz, B., and Prahl, J., “Parched Elasto Hydrodynamic Lubrication Film Thickness Measurement in an Instrument Ball Bearing,” *Tribology Transactions*, **33**, 1, 11-14, (1990).

26) Kingsbury, E., “Ball Contact Locus in an Angular Contact Bearing,” *J. Lubr. Tech.*, **105**, 2, 166-170, (1983).

27) Kingsbury, E., “Ball Motion Perturbation in an Angular Contact Ball Bearing,” *ASLE Trans*., **25**, 3, 279-282, (1982).

28) Hunter, S., Kingsbury, E., and Prahl, J., “Oil Film Thickness and Analysis for an Angular Contact Ball Bearing Operating in Parched Elastohydrodynamic Lubrication,” *Proc. Inst. Mech. Eng. (London),Tribology-Friction, Lubrication and Wear*, **I**, 81-84, (1987).

29) Olsen, A.J. “Load Carrying Capacity Between Lubricated Counter Rotating Balls,” Masters of Science Thesis, Massachusetts Institute of Technology, (1990).

30) Schritz, B. Jones, W.R., Jr., Prahl, J., and Jansen,R., “Parched Elastohydrodynamic Lubrication: Instrumentation and Procedure,” *Trib. Trans*., **37**, 1, 13-22, (1994).

31) DeLucie, D. “Load Carrying Capacity of Counter Rotating Balls in a Retainerless Bearing,” Masters of Science Thesis, Massachusetts Institute of Technology, (1992).

32) Jones, W.R., Jr., Shogrin, B.A., and Kingsbury, E.P., “Long Term Performance of a Retainerless Bearing Cartridge With an Oozing Flow Lubricator for Spacecraft Applications,” 4th International Rolling Element Bearing Symposium, Orlando Florida April 1997, NASA-TM 107492, (Aug. 1997).

33) Jones, W.R., Jr., Toddy, T.J., Predmore, R., Shogrin, B., and Herrera-Fierro, P., “The Effect of ODC-Free Cleaning Techniques on Bearing Lifetimes in the Parched Elastohydrodynamic Regime,” 2nd Aerospace Environmental Technology Conference, Huntsville, Alabama, Aug. 1996, NASA-TM 107322, (Sept. 1996).

34) Shogrin, B.A., "Experimental Determination of Load Carrying Capacity of Point Contacts at Zero Entrainment Velocity," Dissertation, Case Western Reserve University, Cleveland Ohio, (1998).

35) Shogrin, B.A., "Development of a Versatile EHL Tribometer," In process, to be submitted to STLE.

36) Precision Bearings, SKF Catalogue 3700/IE, Weppert GmbH & Co., Germany, (1991).

37) NYE Data Sheets and Product Bulletins, (1997).

38) Johnston, G.J., Wayte, R. and Spikes, H.A., "The Measurement and Study of Very Thin Lubricant Films in Concentrated Contacts," *Tribology Transactions*, **34**, 2, 187-194, (1991).

39) Dyson, A., Naylor, H., and Wilson, A.R. "The Measurement of Oil-Film Thickness in Elastohydrodynamic Contacts," *Proc. Instn Mech Engrs*, Part 3B,**180**,119-134,(1965-66).

40) Allen, G.E., Peacock, L.A., and Rhoads, W.L., "Measurement of Lubricant Film Thickness in Hertzian Contacts," NASA-CR105378, (1968).

41) Woodwell, R.G., Miller, L., and Anderson, C., "Alkaline Cleaning: Its Effects on Tricresyl Phosphate Coated Bearing Steels," *Proceedings of Non-Ozone Depleting Chemical Cleaning and Lubrication of Space System Mechanical Components for Multi-Year Operations*, Denver, CO, (Sept. 1994).

42) Ashby, M.F., Abulawi, J., and Kong, H.S., "Temperature Maps for Frictional Heating in Dry Sliding," *Tribology Transactions*, **34**, 4, 577-587, (1991).

43) Allen, C.M. and Drauglis, E., "Boundary Layer Lubrication:Monolayer or Multilayer," *Wear*, 14, 363-384, (1969).

44) Needs, S.J., "Boundary Film Investigations," *Trans. ASME*, **62**, 331, (1940).

45) Fuks, G.I., "The Properties of Solutions of Organic Solids in Liquid Hydrocarbons at Solid Surfaces," in B. V.. Deryagin (ed.), *Research in Surface Forces*, **1**, (1960).

46) Georges, J.M., Millot, S., Loubet, J.L., and Tonck, A., "Drainage of Thin Liquid Films Between Relatively Smooth Surfaces," *J. Chem. Phys.*, **98**, 9, (May 1993).

47) Israelachvili, J.N. "Measurements and Relation Between the Dynamic and Static Interactions Between Surfaces Separated by Thin Liquid and Polymer Films," *Pure and Applied Chemistry*, **60**, 1473-1478, (1988).

48) Cann, P.M. and Spikes, H.A., "The Behavior of Polymer Solutions in Concentrated Contacts: Immobile Surface Layer Formation," *Tribology Transactions*, **37**, 3, 580-586, (1994).

49) Smeeth, M., Spikes, H.A., and Gunsel, S., "The Formation of Viscous Surface Films by Polymer Solutions: Boundary or Elastohydrodynamic Lubrication?," *Tribology Transactions*, **39**, 3, 720-725, (1996).

50) Guangteng, G. and Spikes, H., "Fractionation of Liquid Lubricants at Solid Surfaces," *Wear*, **200**, 336-345, (1996).

Table 4. Running conditions for the zero entrainment velocity tests.

Test #	Sliding Speed (shaftrps)	Approach Velocity (Voltage Increment)	C [pF] (Cons.#)	R [Ω] (Cons.#)	D [-] (Cons.#)	Bath Temp [°C]	Mensc Temp [°C]
1z	5.0 m/s (12.5 rps)	2.3 μm/sec	24 pF (1)	500 Ω (1)	1.0 (1)	35 °C	35 °C
2z	6.0 m/s (15.0 rps)	2.3 μm/sec	24 pF (1)	500 Ω (1)	1.0 (1)	35 °C	35 °C
3z	6.0 m/s	0.64 μm/sec	24 pF (1)	500 Ω (1)	1.0 (1)	35 °C	35 °C
4z	6.0 m/s	0.13 μm/sec	24 pF (1)	500 Ω (1)	1.0 (1)	35 °C	35 °C
5z	6.0 m/s	0.051 μm/sec	24 pF (1)	500 Ω (1)	1.0 (1)	35 °C	35 °C
6z	6.0 m/s	0.051 μm/sec	24 pF (1)	500 Ω (1)	1.0 (1)	35 °C	37 °C
7z	6.0 m/s	0.053 μm/sec	26 pF (1)	5000 Ω (1)	3.0 (1)	35 °C	37 °C
8z	6.0 m/s	0.051 μm/sec	37 pF (1)	5000 Ω (1)	5.0 (1)	35 °C	40 °C
9z	6.0 m/s	0.048 μm/sec	37 pF (1)	5000 Ω (1)	5.0 (1)	35 °C	40 °C
10z	6.0 m/s	0.051 μm/sec	37 pF (1)	5000 Ω (1)	5.0 (1)	35 °C	40 °C
11z	6.0 m/s	0.053 μm/sec	37 pF (1)	10000 Ω (1)	5.0 (1)	35 °C	40 °C
12z	6.0 m/s	0.056 μm/sec	37 pF (1)	10000 Ω (1)	5.0 (1)	35 °C	40 °C
13z	6.0 m/s	0.058 μm/sec	40 pF (1)	30000 Ω (1)	5.0 (1)	35 °C	40 °C
14z	6.0 m/s	0.053 μm/sec	40 pF (1)	40000 Ω (1)	5.0 (1)	35 °C	45 °C
15z	6.0 m/s	0.046 μm/sec	40 pF (1)	40000 Ω (1)	5.0(1)	40 °C	45 °C
16z	6.0 m/s	0.064 μm/sec	35 pF (2)	20000 Ω (2)	5.0 (3)	35 °C	40 °C
17z	6.0 m/s	0.064 μm/sec	35 pF (2)	20000 Ω (2)	5.0 (3)	35 °C	40 °C
18z	6.0 m/s	0.053 μm/sec	35 pF (3)	20000 Ω (3)	5.0 (3)	40 °C	45 °C
19z	6.0 m/s	0.058 μm/sec	35 pF (5)	20000 Ω (5)	5.0 (5)	40 °C	45 °C
20z	6.0 m/s	0.051 μm/sec	35 pF (5)	20000 Ω (5)	5.0 (5)	50 °C	50 °C
21z	8.0 m/s (20.0 rps)	0.066 μm/sec	35 pF (5)	20000 Ω (5)	5.0 (5)	50 °C	50 °C
22z	10.0 m/s (25.0 rps)	0.076 μm/sec	35 pF (5)	20000 Ω (5)	5.0 (5)	50 °C	50 °C
23z	8.0 m/s (20.0 rps)	0.053 μm/sec	35 pF (5)	20000 Ω (5)	5.0 (5)	50 °C	50 °C
24z	3.0 m/s (7.5 rps)	0.058 μm/sec	35 pF (5)	20000 Ω (5)	5.0 (5)	50 °C	50 °C
25z	1.0 m/s (2.5 rps)	0.060 μm/sec	35 pF (5)	20000 Ω (5)	5.0 (5)	50 °C	50 °C

NOMENCLATURE

A_{hertz}	Hertzian area, m^2
C_{total}	Total measured capacitance, $C_{hertz} + C_{meniscus}$, F
C_{hertz}	Capacitance of Hertzian region, F
$C_{meniscus}$	Capacitance of meniscus region, F
h_{cent}	Theoretical central film thickness, m
h_{min}	Theoretical minimum film thickness, m
h_{film}	Film thickness approximation, m
R_a	Arithmetic surface roughness, m
r_{hertz}	Hertzian radius, m
u	Entrainment velocity, $(u_1+u_2)/2$, m/s
u_1, u_2	Surface velocity, m/s
α	Pressure viscosity coefficient, m^2/N
ε_{atm}	Dielectric constant of lubricant at atmospheric pressure
ε_{hertz}	Dielectric constant of lubricant at Hertzian pressure
σ_{max}	Maximum Hertzian contact stress, N/m^2
κ	Coulomb's constant, 8.9875×10^9 $[(N*m^2)/C^2]$
Λ	Lambda value
η_o	Dynamic atmospheric viscosity, Ns/m^2
ZEV	Zero entrainment velocity

Table 1. Selected properties of the test lubricant.[37]

Kinematic viscosity at 24 °C 40 °C 80 °C 120 °C	127.3 mm^2s^{-1} 59.7 mm^2s^{-1} 15.57 mm^2s^{-1} 6.53 mm^2s^{-1}
Density at 24 °C 40 °C 80 °C 120 °C	0.830 gcm^{-3} 0.819 gcm^{-3} 0.793 gcm^{-3} 0.767 gcm^{-3}
Dielectric Breakdown Voltage*	13.8 Volts/μm

* Dielectric Breakdown Voltage value is that of PAO-176.[37]

Table 2. Effective pressure-viscosity coefficients, α_{EFF}, at four temperatures.[38]

Test Temperature	Effective Pressure Viscosity Coefficient
24 °C	20.5 GPa^{-1}
40 °C	19.0 GPa^{-1}
80 °C	14.5 GPa^{-1}
120 °C	11.0 GPa^{-1}

Table 3. Running conditions for pure rolling tests.

Test #	Max. Hertzian Contact Stress (GPa)	Approx. Running Time	First Entrainment Velocity (shaft rps)	Second Entrainment Velocity (shaft rps)	Third Entrainment Velocity (shaft rps)	Data Sets Collected
2rwos	0.64	400 sec	2.0 m/s (10.0 rps)	-	-	1320
3rwos	0.63	450 sec	2.5 m/s (12.5 rps)	3.0 m/s (15.0 rps)	2.0 m/s	1580
4rwos	0.64	500 sec	3.0 m/s	2.0 m/s	2.5 m/s	
	0.82	400 sec.	2.5 m/s	2.0 m/s	3.0 m/s	3050 (combined)
5rwos	0.81	600 sec	2.5 m/s	3.0 m/s	2.0 m/s	2010
6rwos	0.81	500 sec	2.0 m/s	2.5 m/s	1.5 m/s (7.5 rps)	1590
7rwos	1.01	500 sec	2.5 m/s	2.0 m/s	3.0 m/s	1650

Table 5. Capacitance and film thickness results for the dynamically loaded roll without slip tests.

Table Key

Entrainment Velocity $Capacitance_{mean}$ ($Capacitance_{StandDev}$) [number of data points] h_{mean} ($h_{StandDev}$) ($minimum_{24C}$) ($central_{24C}$)			
Max. Hertzian Stress (GPa) [test #]			
0.64 [2rwos]	2.0 m/s 15.5 pF (0.4 pF) [891] 0.78 μm (0.11 μm) (0.58 μm) (0.99 μm)	-	-
0.63 [3rwos]	2.5 m/s 14.4 pF (0.3 pF) [240] 1.08 μm (0.12 μm) (0.68 μm) (1.16 μm)	3.0 m/s 14.0 pF (0.3 pF) [245] 1.24 μm (0.15 μm) (0.77 μm) (1.31 μm)	2.0 m/s 15.8 pF (0.5 pF) [480] 0.70 μm (0.10 μm) (0.59 μm) (1.00 μm)
0.64 [4rwos]	3.0 m/s 14.0 pF (0.4 pF) [450] 1.27 μm (0.174 μm) (0.77 μm) (1.30 μm)	2.0 m/s 16.0 pF (0.3 pF) [385] 0.67 μm (0.06 μm) (0.58 μm) (0.99 μm)	2.5 m/s 15.7pF (0.4 pF) [620] 0.74 μm (0.08 μm) (0.67 μm) (1.15 μm)
0.82 [4rwos cont.]	2.5 m/s 16.9 pF (0.3 pF) [235] 0.69 μm (0.04 μm) (0.64 μm) (1.10 μm)	2.0 m/s 18.4 pF (0.4 pF) [270] 0.53 μm (0.04 μm) (0.55 μm) (0.94 μm)	3.0 m/s 16.5 pF (0.5 pF) [385] 0.75 μm (0.07 μm) (0.73 μm) (1.24 μm)
0.81 [5rwos]	2.5 m/s 16.7 pF (0.3 pF) [260] 0.72 μm (0.05 μm) (0.64 μm) (1.10 μm)	3.0 m/s 15.8 pF (0.5 pF) [540] 0.87 μm (0.10 μm) (0.73 μm) (1.24 μm)	2.0 m/s 18.0 pF (0.3 pF) [562] 0.56 μm (0.03 μm) (0.55 μm) (0.94 μm)
0.81 [6rwos]	2.0 m/s 17.1 pF (0.5 pF) [490] 0.67 μm (0.07 μm) (0.55 μm) (0.94 μm)	2.5 m/s 16.4 pF (0.4 pF) [270] 0.77 μm (0.07 μm) (0.64 μm) (1.10 μm)	1.5 m/s 19.0 pF (0.2 pF) [249] 0.49 μm (0.02 μm) (0.45 μm) (0.78 μm)
1.01 [7rwos]	2.5 m/s 18.4 pF (0.3 pF) [280] 0.70 μm (0.03 μm) (0.61 μm) (1.05 μm)	2.0 m/s 20.0 pF (0.4 pF) [325] 0.57 μm (0.03 μm) (0.53 μm) (0.90 μm)	3.0 m/s 17.9 pF (0.6 pF) [305] 0.76 μm (0.07 μm) (0.69 μm) (1.18 μm)

Table 6. Summary of the most successful zero entrainment tests.

Test #	Sliding Speed	Contact Stress	Amount of Time Spent in Contact	IR Temp Rise <Oil Bath Temp Rise>	[# of data points] C_{mean} ($C_{StandDev}$) h_{mean} ($h_{StandDev}$)	Surpassed Limit Criteria (Actual Value(s))
22z	10.0m/s	≤0.52GPa	28.8 min	22 °C <6 °C>	[4311] 21.8 pF (1.1 pF) 0.143 μm (0.018 μm)	Voluntary Shutdown
23z	8.0m/s	≤0.57GPa	28.2 min	28 °C <7 °C>	[4250] 22.5 pF (1.2 pF) 0.143 μm (0.020 μm)	IR Temperature 50 °C (1X) (50 °C)
21z	8.0m/s	≤0.46GPa	26.7 min	21 °C <5 °C>	[3925] 21.7 pF (1.1 pF) 0.136 μm (0.017 μm)	Voluntary Shutdown
19z	6.0m/s	≤0.35GPa	17.5 min	19 °C <3 °C>	[2390] 22.1 pF (1.2 pF) 0.090 μm (0.022 μm)	IR Temperature 45 °C (1X) (45 °C)
20z	6.0m/s	≤0.45GPa	24.3 min	21 °C <6 °C>	[3350] 22.6 pF (1.5 pF) 0.107 μm (0.025 μm)	Capacitance 35 pF (5X) (604 pF, 96.1 pF, -51.2 pF,-558 pF, 99.4 pF)

Table 7. Other successful zero-entrainment tests.

Test #	Sliding Speed	Contact Stress	Amount of Time Spent in Contact	IR Temp Rise <Oil Bath Temp Rise>	Surpassed Limit Criteria (Actual Value(s))
18z	6.0 m/s	≤ 0.35 GPa	575 sec	15 °C <2 °C>	Dissipation 5.0 (3X) (7.0, 9.3, 17.5)
17z	6.0 m/s	≤ 0.3 GPa	110 sec	8 °C <2 °C>	Capacitance 35 pF (2X) (40.3 pF, -37.0 pF)
16z	6.0 m/s	≤ 0.35 GPa	180 sec	8 °C <2 °C>	Capacitance 35 pF (2X) (100.1 pF, -353.8 pF)
5z	6.0 m/s	≤ 0.2 GPa	45 sec	6 °C <2 °C>	Capacitance 24 pF (1X) (35.5 pF) and Dissipation 1.0 (1X) (1.4)
8z	6.0 m/s	≤ 0.2 GPa	110 sec	7 °C <1 °C>	Capacitance 37 pF (1X) (52.5 pF)
10z	6.0 m/s	≤ 0.2 GPa	190 sec	10 °C <2 °C>	Dissipation 5.0 (1X) (26.9)
11z	6.0 m/s	≤ 0.15 GPa	15 sec	7°C <1°C>	Capacitance 37 pF (1X) (325.0 pF)
9z	6.0 m/s	≤ 0.15 GPa	100 sec	8 °C <2 °C>	Capacitance 37 pF (1X) (-568.0 pF)
15z	6.0 m/s	≤ 0.15 GPa	70 sec	6 °C <1 °C>	Capacitance 40 pF (1X) (127.0 pF)

Table 8. Summary of sustained load carrying capacity as a function of contact stress and sliding speed for zero entrainment tests.

Test #	Sliding Speed	Contact Stress	Amount of Time Spent in Contact	Surpassed Limit Criteria (Actual Value(s))
22z	10.0m/s	≤0.52 GPa	28.8 min	Voluntary Shutdown
21z	8.0m/s	≤0.46 GPa	26.7 min	Voluntary Shutdown
20z	6.0m/s	0.45 GPa	24.3 min	Capacitance 35 pF (5X) (604 pF, 96.1 pF, -51.2 pF,-558 pF, 99.4 pF)
24z	3.0m/s	0.36 GPa	3.5 min	Dissipation 5.0 (5X) (6.0, 12.7, 16.2, 214.5, 102.2)
25z	1.0m/s	<0.15 GPa	< 4.0 sec	Capacitance 35 pF (5X) (-10434.7 pF, 1397.7 pF, 27655.9 pF, 43414.7 pF, 26414.9 pF) Resistance 20,000 Ω (5X) (-27.7 Ω, 26.8 Ω, -18.4 Ω, -17.2 Ω, -31.3 Ω) Dissipation 5.0 (5X) (55.1, 424.1, 31.3, 21.3, 19.3)

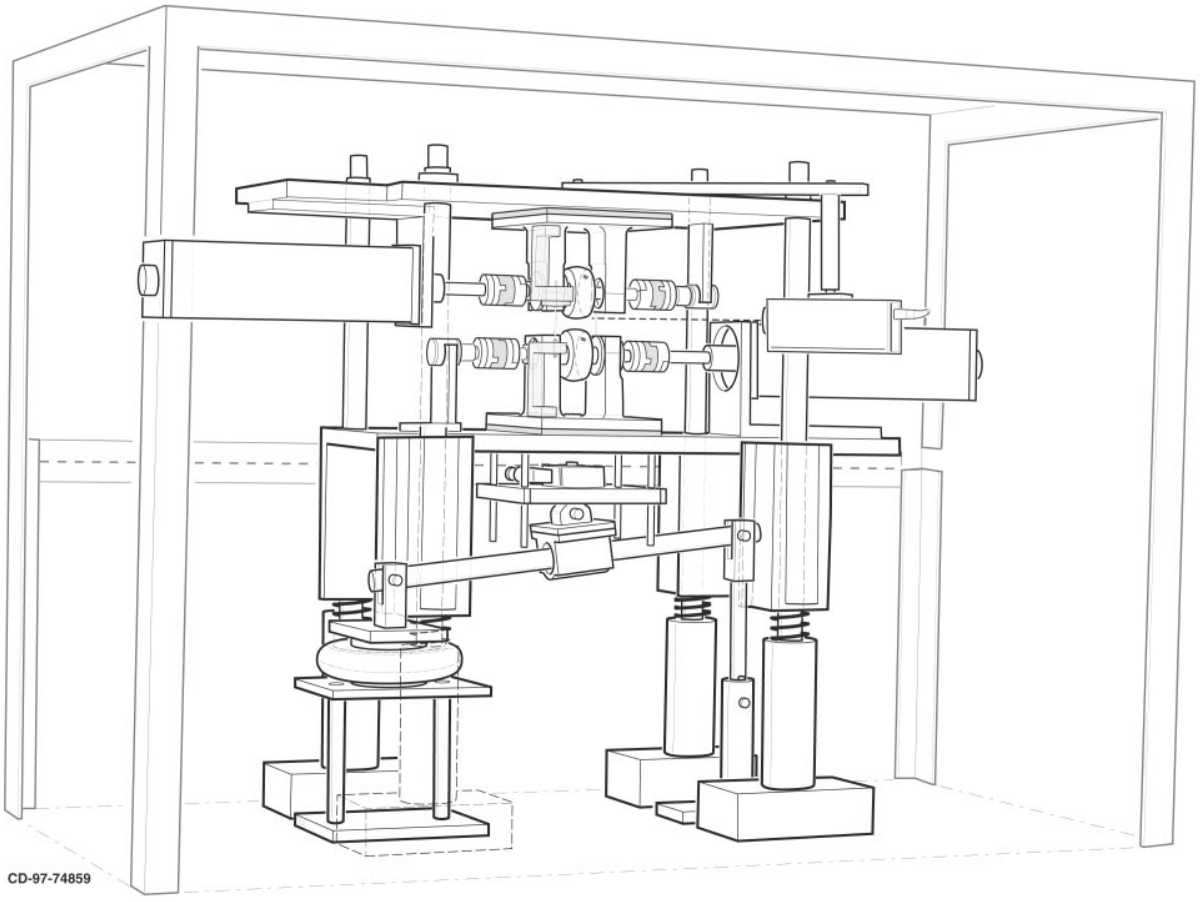

Figure 1. Overall View of Tribometer

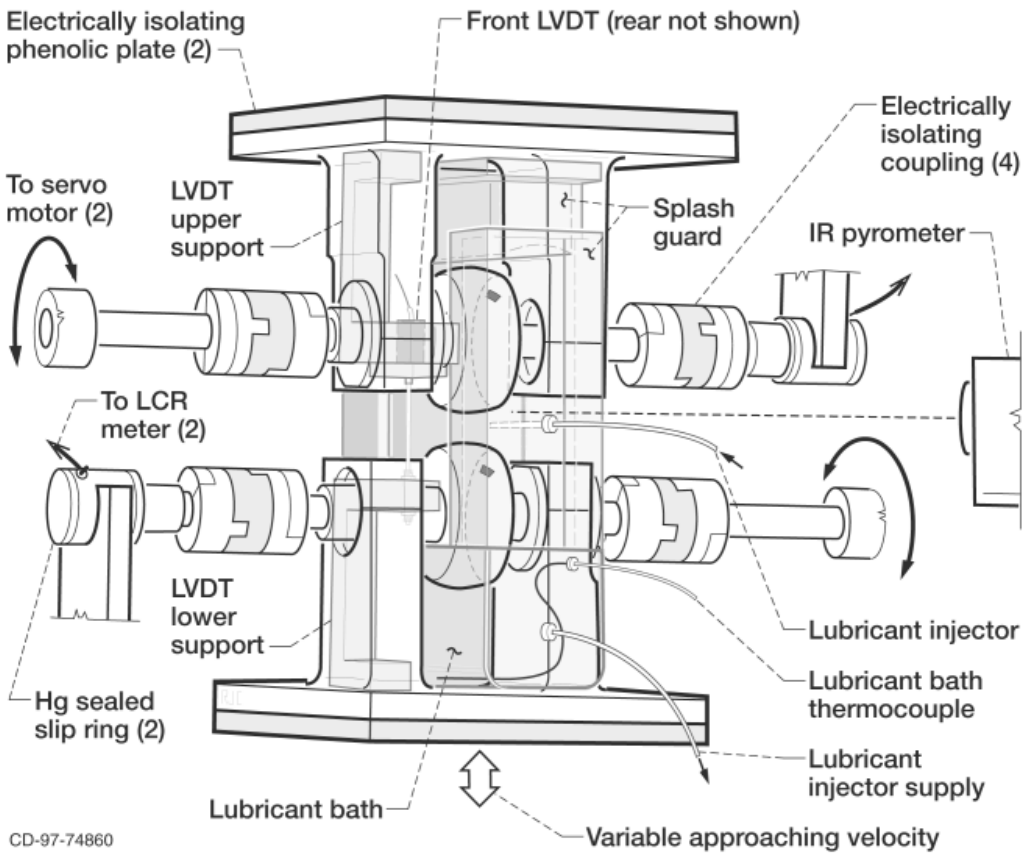

Figure 2. Detailed view of specimens and surrounding mechanisms

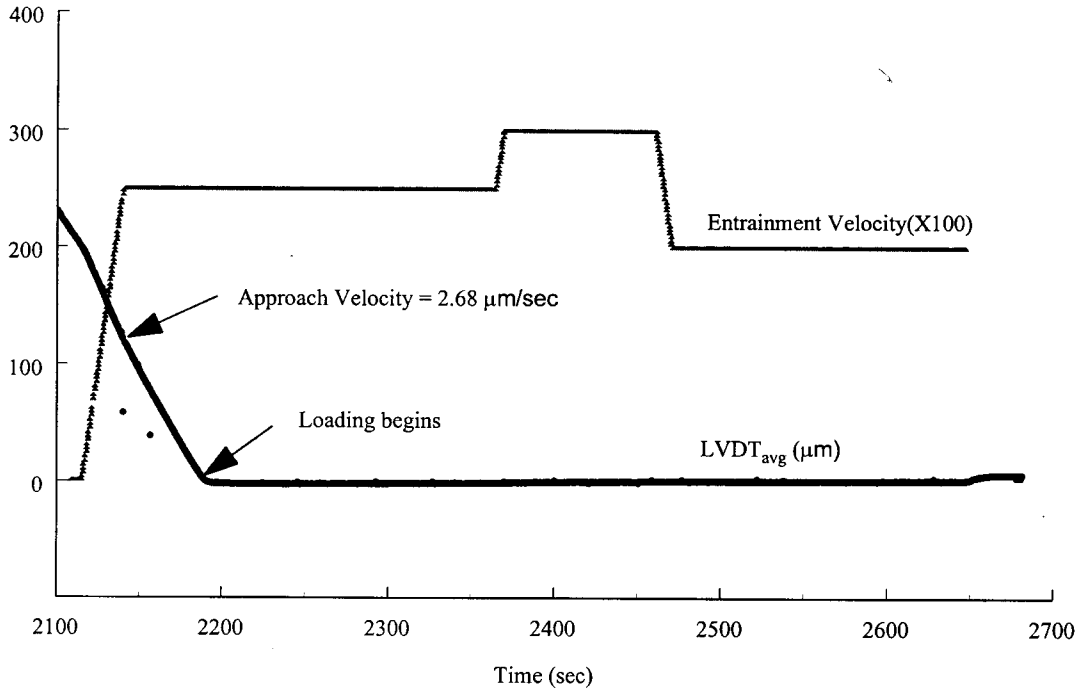

Figure 3. Ball-ball approach and entrainment velocity (x100) for pure rolling test '3rwos'

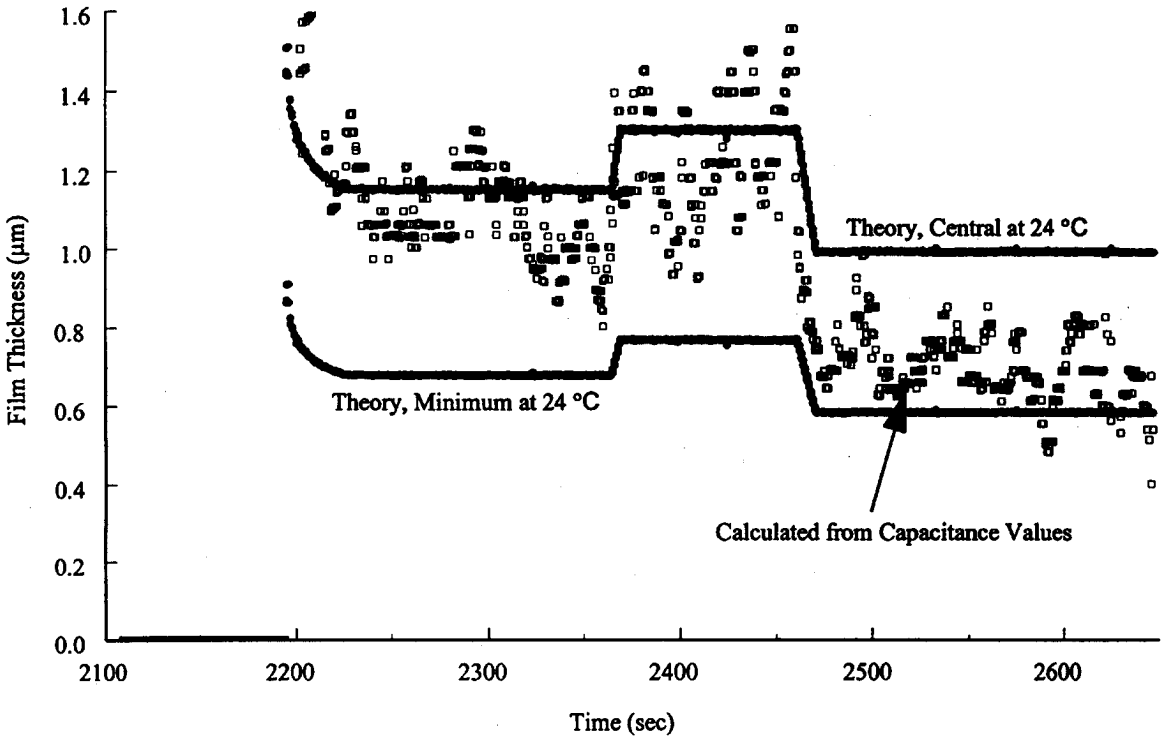

Figure 4. Comparison between theoretical and experimental approximated film thickness for roll without slip test '3rwos'

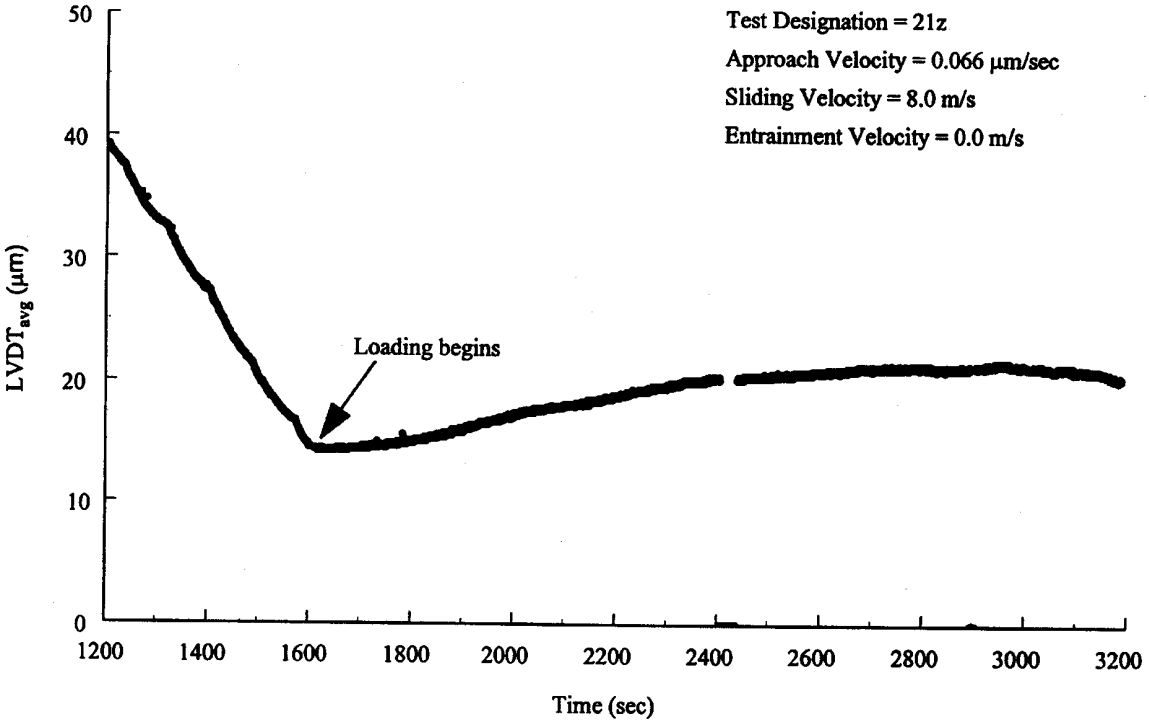

Figure 5. Ball-ball final approach for zero entrainment velocity test '21z'

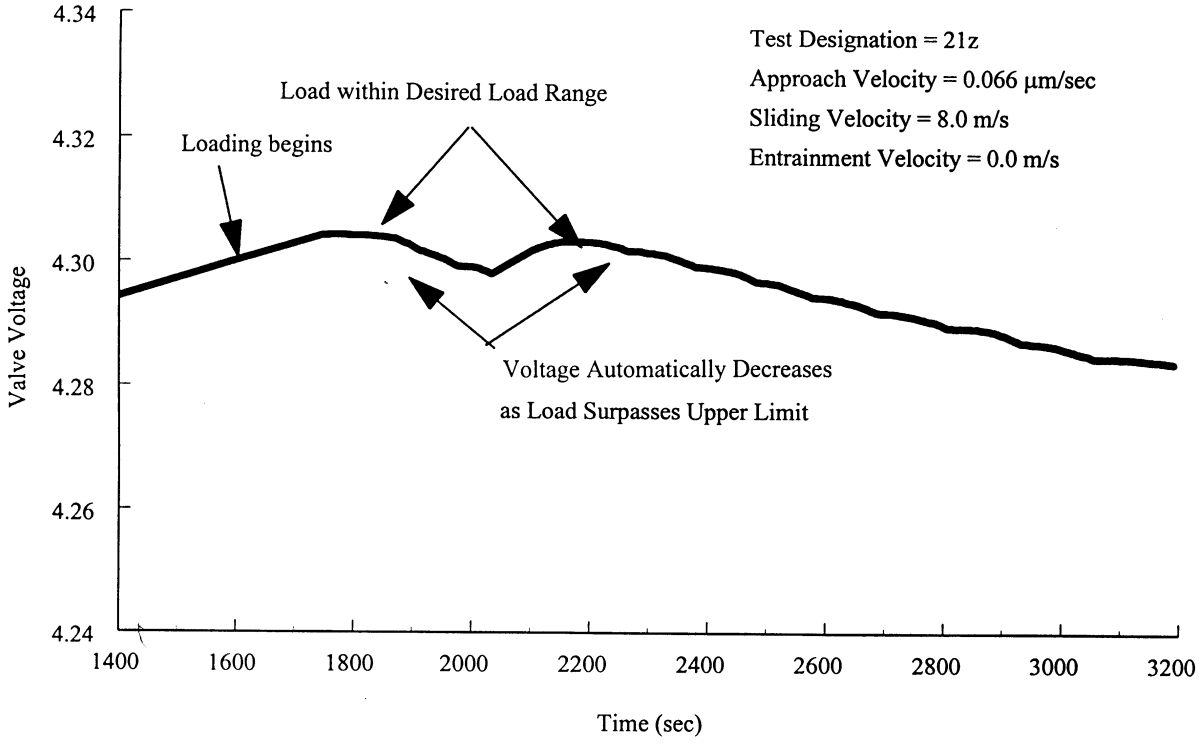

Figure 6. Proportional valve voltage during zero entrainment velocity test '21z'

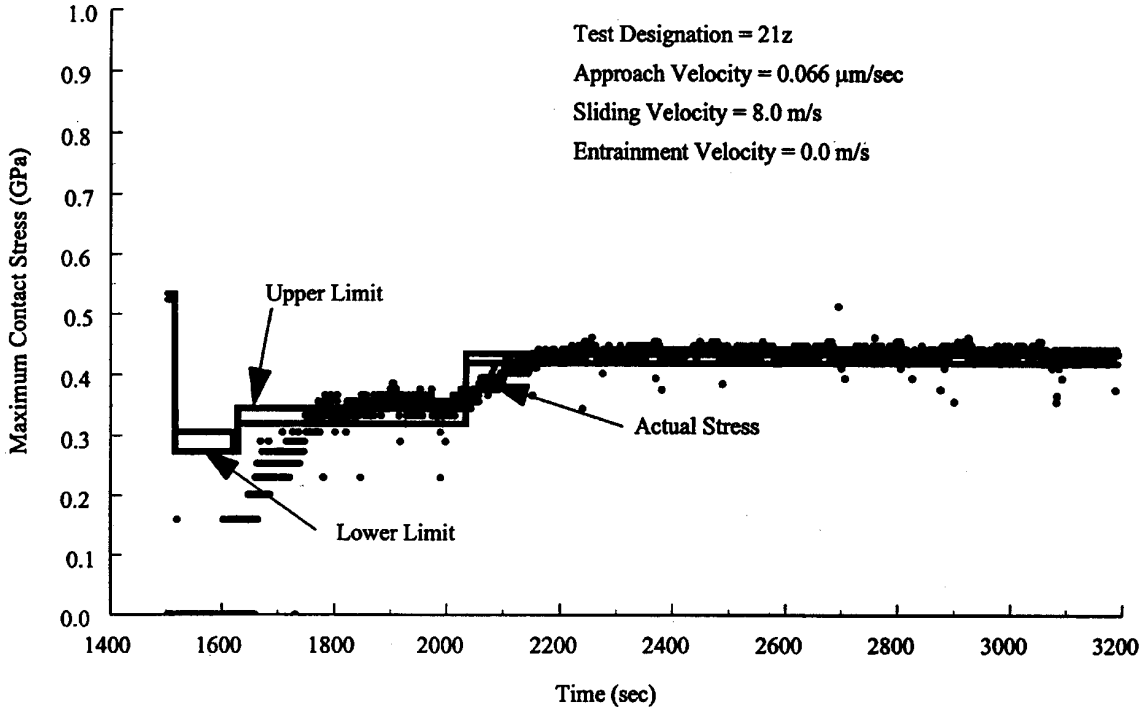

Figure 7. Actual and desired maximum Hertzian contact stress for zero entrainment test ‘21z’

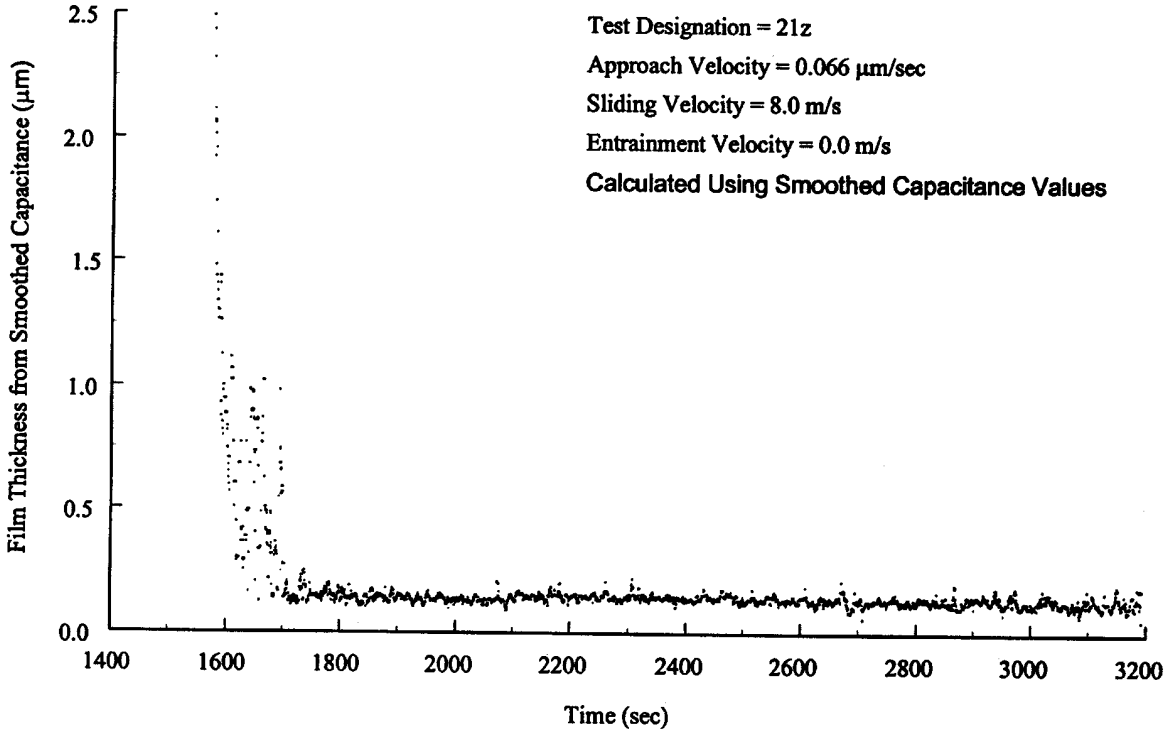

Figure 8. Film thickness approximations for zero entrainment test ‘21z’

REPORT DOCUMENTATION PAGE

Form Approved
OMB No. 0704-0188

1. AGENCY USE ONLY (*Leave blank*)	2. REPORT DATE	3. REPORT TYPE AND DATES COVERED
	January 1999	Technical Memorandum

4. TITLE AND SUBTITLE

Experimental Determination of Load Carrying Capacity of Point Contacts at Zero Entrainment Velocity

5. FUNDING NUMBERS

WU–274–00–00–00

6. AUTHOR(S)

Bradley A. Shogrin, William R. Jones, Edward P. Kingsbury, and Joseph M. Prahl

7. PERFORMING ORGANIZATION NAME(S) AND ADDRESS(ES)

National Aeronautics and Space Administration
Lewis Research Center
Cleveland, Ohio 44135–3191

8. PERFORMING ORGANIZATION REPORT NUMBER

E–11469

9. SPONSORING/MONITORING AGENCY NAME(S) AND ADDRESS(ES)

National Aeronautics and Space Administration
Washington, DC 20546–0001

10. SPONSORING/MONITORING AGENCY REPORT NUMBER

NASA TM—1999-208848

11. SUPPLEMENTARY NOTES

Bradley A. Shogrin, Case Western Reserve University, Cleveland, Ohio, (work funded under cooperative agreement NCC3–409, presently with Space Systems/Loral); William R. Jones, Jr., NASA Lewis Research Center; Edward P. Kingsbury, IRC, Walpole, Massachusetts; Joseph M. Prahl, Case Western Reserve University, Cleveland, Ohio, (work funded under cooperative agreement NCC3–409). Responsible person, William R. Jones, Jr., organization code 5140, (216) 433–6051.

12a. DISTRIBUTION/AVAILABILITY STATEMENT

Unclassified - Unlimited
Subject Category: 34 Distribution: Nonstandard

This publication is available from the NASA Center for AeroSpace Information, (301) 621–0390.

12b. DISTRIBUTION CODE

13. ABSTRACT ***(Maximum 200 words)***

A capacitance technique was used to monitor the film thickness separating two steel balls of a unique tribometer while subjecting the ball-ball contact to highly stressed, zero entrainment velocity (ZEV) conditions. All tests were performed under a N_2 purge (R.H. < 1.0%) and utilized 52100 steel balls (R_a = 0.02 mm). Tribometer operations and capacitance-to-film-thickness accuracy were verified by comparing the film thickness approximations to established theoretical predictions for test conditions involving pure rolling. Pure rolling experiments were performed under maximum contact stresses and entrainment velocities of £ 1.0 GPa and 1.0 m/s to 3.0 m/s, respectively. All data from these baseline tests conformed to theory. ZEV tests were initiated after calibration of the tribometer and verification of film thickness approximation accuracy. Maximum contact stresses up to 0.57 GPa were supported at zero entrainment velocity with sliding speeds from 6.0 to 10.0 m/s for sustained amounts of time up to 28.8 minutes. The protective lubricating film separating the specimens at ZEV had a thickness between 0.10 and 0.14 mm (4 to 6 min), which corresponds to an approximate L-value of 4. The film thickness did not have a strong dependence upon variations of load or speed. Decreasing the sliding speed from 10.0 m/s to 1 m/s revealed a rapid loss in load support between 3.0 and 1.0 m/s. The formation of an immobile film formed by lubricant entrapment is discussed as an explanation of the load carrying capacity at these zero entrainment velocity conditions, relevant to the ball-ball contact application in retainerless ball bearings.

14. SUBJECT TERMS

Tribology; Retainerless bearings

15. NUMBER OF PAGES

38

16. PRICE CODE

A03

17. SECURITY CLASSIFICATION OF REPORT	18. SECURITY CLASSIFICATION OF THIS PAGE	19. SECURITY CLASSIFICATION OF ABSTRACT	20. LIMITATION OF ABSTRACT
Unclassified	Unclassified	Unclassified	